https://doi.org/10.5194/egusphere-2022-709
Preprint. Discussion started: 10 August 2022

River incision, ^{10}Be production and transport in a source-to-sink sediment system (Var catchment, SW Alps)

Carole Petit[1], Tristan Salles[2], Vincent Godard[3], Yann Rolland[4,5], and Laurence Audin[5]

[1]Université Côte d'Azur, CNRS, Observatoire de la Côte d'Azur, IRD, Géoazur, 250 rue Albert Einstein, Sophia Antipolis 06560 Valbonne, France
[2]School of Geosciences, The University of Sydney, Sydney, NSW 2006, Australia
[3]Aix-Marseille Université, CNRS, Coll France, IRD, INRAE, CEREGE, Aix en Provence, France
[4]EDYTEM, Université Savoie Mont Blanc, CNRS, UMR 5204, Le Bourget du Lac, France
[5]5 ISTerre, Université Grenoble Alpes, Univ. Savoie Mont Blanc, CNRS, IRD, IFSTTAR, 38000 Grenoble, France

Correspondence: Carole Petit (carole.petit@univ-cotedazur.fr)

Abstract. Detrital ^{10}Be from continental river sands or submarine sediments has been extensively used to determine the average long-term denudation rates of aerial catchments, based on the assumption that the rate of cosmonuclide production by interaction of source rocks with cosmic radiations balances out the loss of these elements by surface denudation. However, the ^{10}Be signal of in-situ produced sediments may be altered by the response time of mountainous catchments to high-frequency forcings; besides, transient sediment storage in piedmonts, alluvial plains, lakes or near the coast may also induce a difference between the erosive signal and its record in the sedimentary sink. Consequently, a significant part of the signal recorded in shallow-water sediments can be lost, as deep marine sediments may record simultaneously a signal coming from newly eroded source rocks along with one coming from the destabilization of previously deposited sediments.

In this paper, we use the Surface Process Model Badlands to simulate erosion, deposition and detrital ^{10}Be transfer from a source-to-sink sedimentary system (the Var River catchment, Southern French Alps) over the last 100 kyr. We first compare real denudation rates with the ones that would be extracted from in-situ produced sediments and from off-shore deposited sediments over time in order to examine how the ^{10}Be record in sediments provides an accurate estimate of continental denudation rates. Then, we examine which conditions (precipitation rate, flexure, ice cover) permit to satisfy published measured river incision rates and ^{10}Be concentration in submarine sediments.

Our results, based on the Var catchment cosmic ray exposure dating and modelling indicate that, while river sands do accurately estimate the average denudation rate of continental catchments, it is much less the case for submarine deep sea sediments. We found that deep sea sediments have a different, and often much noisier ^{10}Be signature than continental ones, and record a significant time lag with respect to actual precipitation rate changes, representing the geomorphological response of the margin. The model which best fits both measured ^{10}Be concentration in marine sediments and river incision rates on-land involves an increase in precipitation rates from 0.3 to 0.7 $\mathrm{m.yr}^{-1}$ after 20 ka, hence suggesting more intense precipitations starting at the end of the Last Glacial Maximum.

https://doi.org/10.5194/egusphere-2022-709
Preprint. Discussion started: 10 August 2022

1 Introduction

Sedimentary deposits are important archives of the tectonic and climatic history of continents: for instance, the geometry, grain size, mineralogy and geochemical signature of deposits are impacted by changes in environmental conditions (e.g., relative sea level changes, precipitations over geologic time as well as human activities during the Anthropocene (Syvitski et al., 2022)). Provided good enough estimates of the transfer function between these sedimentary records and their external forcings, they can be reliable tools for reconstructing climatic cycles, subsidence curves, or monsoon onset for instance (Bentley et al., 2016; Li et al., 2016; Liu et al., 2016; Wan et al., 2006). However, depending on the considered timescales, the signatures in submarine sediments of some of these external (i.e., climatic or tectonic) forcings affecting aerial catchments depend on a myriad of processes which still remain difficult to extract from the deep sea record. To this end, one would need to evaluate not only how the eroded source responds to specific forcing but also how long and where are temporarily stored detrital sediments, and when are they re-injected into the system and eventually reach their sink.

Concerning the sediment source, mountainous catchments may not be very sensitive to high-frequency forcings, and the response time of these catchments may alter the external signal of in-situ produced sediments (e.g. Armitage et al., 2013; Goren, 2016). Second, transient sediment storage in piedmonts, alluvial plains, lakes or near the coast may induce a large time lag between the external signal and its record in the sedimentary sink (e.g. Blöthe and Korup, 2013; Clift and Giosan, 2014; Malatesta et al., 2018; Phillips and Slattery, 2006; Romans et al., 2016). Depending on considered timescales, the erosive signal itself can be completely buffered by this process (see a complete review in Romans et al. (2016)). Finally, submarine sediments can be reworked by gravitational processes, especially during sea-level falls (Phillips and Slattery, 2006). As a consequence, a significant part of the signal recorded in shallow-water sediments can be lost, whereas deep marine sediments may record simultaneously a signal coming from newly eroded source rocks and another one coming from the destabilization of previously deposited sediments. In addition, relative sea level variations may affect the connectivity between aerial rivers and submarine canyons, therefore limiting from time to time the efficiency of sediment transport in the offshore domain (Fryirs et al., 2007).

Detrital terrestrial cosmogenic nuclides (TCN, mostly ^{10}Be) concentrations from continental river sands or submarine sediments have been extensively used to determine the average long-term denudation rates of aerial catchments, provided enough quartz-bearing rocks outcrop at the surface to give a representative sampling of the whole catchment denudation (Bierman and Steig, 1996; von Blanckenburg, 2005; Lupker et al., 2012; Mandal et al., 2015; Siame et al., 2011; Vanacker et al., 2007). Denudation rate estimates from ^{10}Be concentration in quartz-rich sediments are often based on the assumption that the rate of TCN production by interaction of source rocks with cosmic radiations balances out the loss of these elements by surface denudation (Lal, 1991). If only ^{10}Be production by neutron spallation is considered, this may lead to a few percent underestimation of the true erosion rates (Balco et al., 2008). Denudation rates can vary in time and space, which also questions this steady-state assumption and may lead to under- or over-estimates of the true denudation rates (Bierman and Steig, 1996). Finally, the proportion of the target mineral (i.e., quartz in the case of ^{10}Be) in surface rocks may also vary, which has to be taken into account in order to correctly estimate the total production rate of a given catchment (Bierman and Steig, 1996).

Hence, understanding how detrital ^{10}Be concentrations recorded in submarine sedimentological archives reflect denudation

https://doi.org/10.5194/egusphere-2022-709
Preprint. Discussion started: 10 August 2022

rates at the time of their deposition requires to quantify: i) how fast and where ^{10}Be is produced; ii) how ^{10}Be concentration in produced sediments is representative of average catchment denudation rates at any given spatiotemporal scale and iii) how long it takes for produced ^{10}Be-rich sediments to reach the sedimentary sink.

In this paper, we use the surface process model Badlands (Salles, 2016) to simulate erosion, deposition and detrital ^{10}Be transfer from a source-to-sink sediment system (the Var River catchment, Southern French Alps), which deposited in the Ligurian (Mediterranean) sea domain since 100 ka. We first compare real denudation rates with the ones that would be extracted from in-situ produced sediments and from off-shore deposited sediments at each time step in order to assess at which timescales the steady-state assumption is valid, and how ^{10}Be record in detrital sediments provides an accurate estimate of continental denudation rates. Then, we examine which conditions (precipitation rate, flexure, ice cover) permit to satisfy published river incision rates (Cardinal et al., 2022; Petit et al., 2019; Rolland et al., 2017, 2020; Saillard et al., 2014) and ^{10}Be concentration in marine sediments (named hereafter ^{10}Be$_{MS}$) in this particular, small-scale source-to-sink system (Mariotti et al., 2021).

2 Geomorphological and Geological setting

The Var catchment in Southern French Alps is ideally suited to constrain source-to-sink processes: it is a relatively small catchment (~2800 $\mathrm{km2}$), which encompasses some of the high altitude (~3000 m) summits of the Alpine Mercantour crystalline massif (1). The Var River has three main large tributaries: the Tinée and Vésubie Rivers, which headwaters are in the crystalline massif and the Esteron River, which flows only across the overlying meso-cenozoic sedimentary sequence. The hydric regime of the Var River, dominated by flash floods, is responsible for frequent hyperpycnal flows in the submarine domain (Mulder et al., 1998). The continental floodplain and shelf at the mouth of the Var River are underdeveloped and most detrital sediments are deposited offshore at the foot of the Ligurian margin at depths > -2000 m. The average annual discharge at the mouth of the Var river is ~50 $\mathrm{m2.s^{-1}}$, but it can reach more than 500 $\mathrm{m2.s^{-1}}$ during floods (Mulder et al., 1998). According to Mulder et al. (1998) and Syvitski et al. (2000), the sediment concentration Cs can be obtained from the following expression:

$$C_s = aQ^b \tag{1}$$

where parameters a and b relate the sediment concentration C_s $[M.L^{-3}]$ to mean discharge Q $[L^3.T^{-1}]$ at the river mouth, and have been estimated to ~7.7e-4 and ~1.65 for the Var River, respectively. Modern average denudation rates estimates of the Var River catchment from ^{10}Be measurements in fluvial sediments range between 0.1 and 0.8 $\mathrm{mm.yr^{-1}}$ (Mariotti et al., 2019). Two other coastal rivers flow East of the Var catchment: the Paillon and Roya Rivers, with much smaller drainage areas (258 and 601 $\mathrm{km2}$, respectively).

A previously published paper presented detailed sedimentological and geochemical analyses of sediment cores in the sedimentary ridge located at the outlet of the Var submarine canyon (Bonneau et al., 2016). These analyses revealed a larger frequency of turbidite flows and larger Epsilon-Neodymium (ε) values during the Last Glacial Maximum (LGM), which is interpreted as reflecting more intense erosion, especially in the crystalline massif, and larger sediment production during glacial periods. In these cores, ^{10}Be$_{MS}$ (per gram of quartz) varies between 2e4 and 7e4 $\mathrm{at.g^{-1}}$, which gives average denudation rates of 0.2 to

https://doi.org/10.5194/egusphere-2022-709
Preprint. Discussion started: 10 August 2022

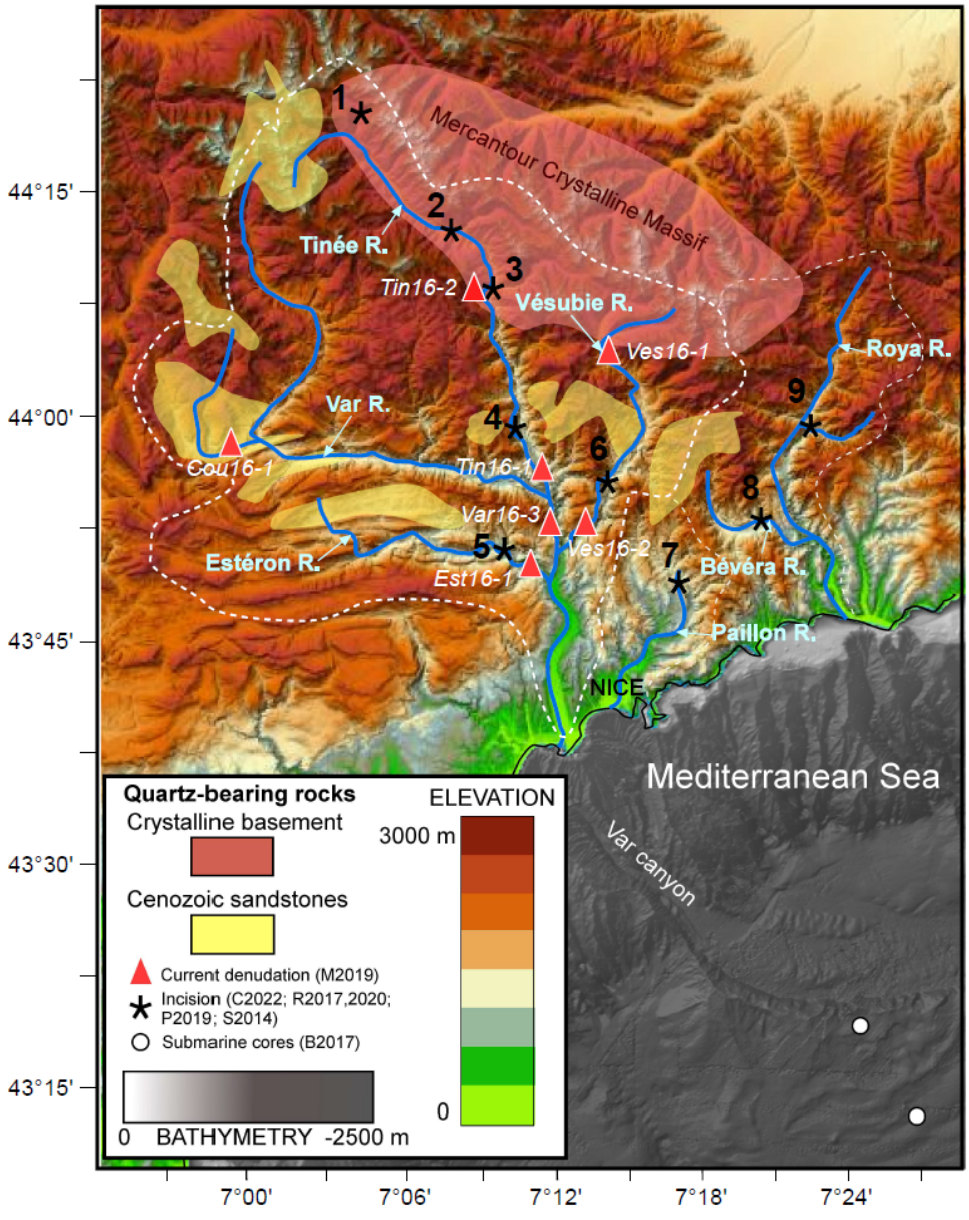

Figure 1. Topographic/bathymetric map and schematic outline of main quartz-bearing rock outcrops of the study area (transparent red and yellow patches). White dashed lines indicate the contours of the Var, Paillon and Roya Rivers catchments. Stars, open dots and triangles indicate the location of data constraints provided by surface exposure dating of river polished surfaces (Saillard et al., 2014; Rolland et al., 2017, 2020; Petit et al., 2019; Cardinal et al., 2022), geochemical analyses of submarine sediments (Bonneau et al., 2017; Mariotti et al., 2021), and detrital ^{10}Be in river sands (Mariotti et al., 2019), respectively. For river polished surfaces, the numbers refer to the following sites: 1 = Salso Moreno; 2 = Isola; 3 = Saint Sauveur; 4 = Lower Tinée; 5 = Estéron; 6 = Vésubie; 7 = Paillon; 8 = Bévéra; 9 = Roya. Italic letters refer to sample names in Mariotti et al. (2019).

https://doi.org/10.5194/egusphere-2022-709
Preprint. Discussion started: 10 August 2022

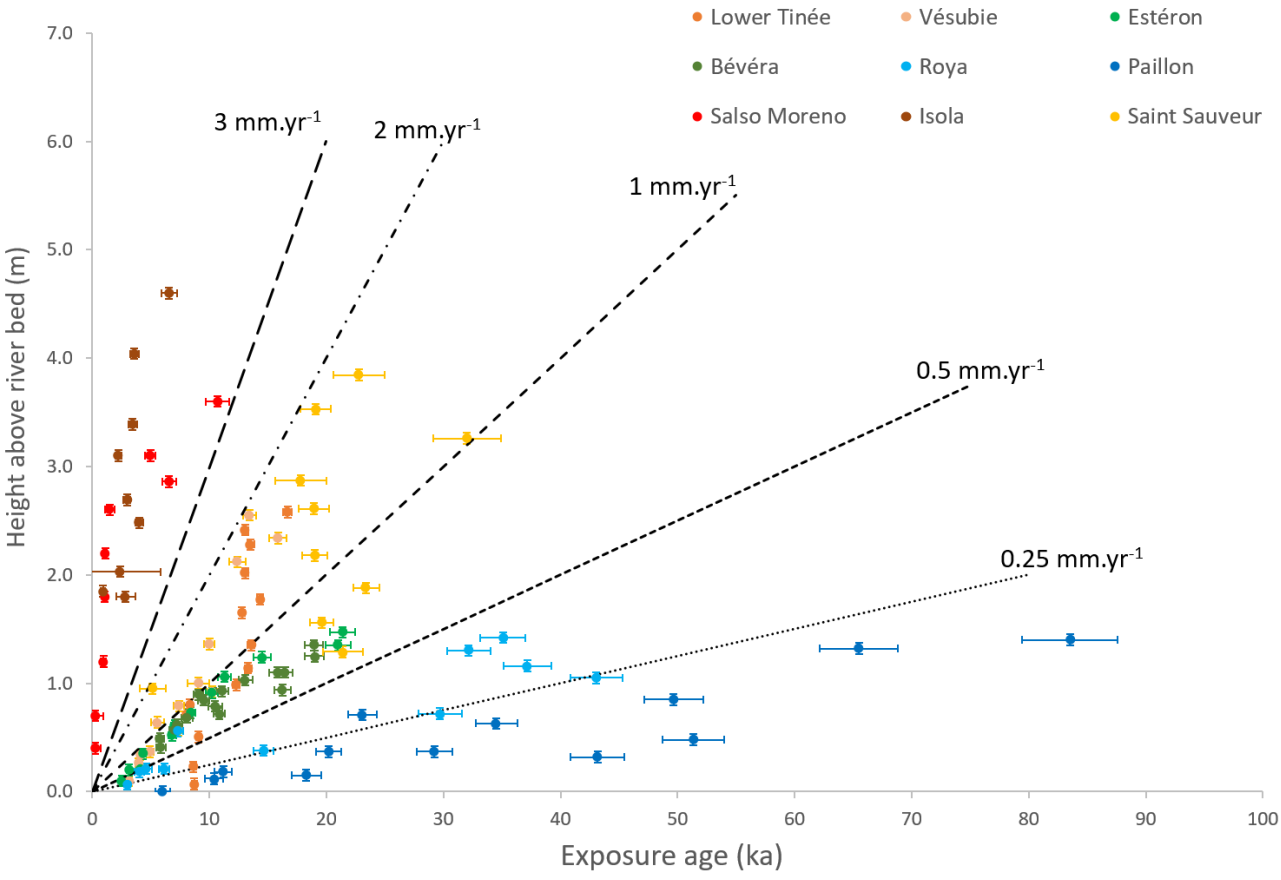

Figure 2. Altitude above the river bed vs. Cosmic Ray Exposure (CRE) ages and corresponding error bars in samples of river-polished surfaces of the Var, Roya and Paillon catchments (Cardinal et al., 2022; Rolland et al., 2020, 2017; Petit et al., 2019; Saillard et al., 2014). See location of the sites on 1. Dashed lines indicate constant incision rate curves, for comparison.

0.5 $\mathrm{mm.yr^{-1}}$ between 70 and 4 ka (Mariotti et al., 2021). On land, Cosmic Ray Exposure (CRE) ages of polished river cliffs have revealed fast incision rates of ~0.5 to 2 $\mathrm{mm.yr^{-1}}$ during the late Pleistocene in most sites of the Var catchment and in the Bévéra River (Cardinal et al., 2022; Petit et al., 2019; Rolland et al., 2017; Saillard et al., 2014). River gorges located at high altitudes in the Mercantour Massif (red-brown dots on 2) show very fast incision (up to 4 $\mathrm{mm.yr^{-1}}$) starting after the Younger Dryas (YD), which can be ascribed to a transient response of formerly glaciated valleys. Most of lower altitude river gorges (3, 4, 5, 6, 8, orange, yellow and green dots on 2) start to be incised around 20 ka (i.e., close to the LGM). Two other sites (7 and 9, blue dots on 2) show much lower incision rates (<0.5 $\mathrm{mm.yr^{-1}}$) extending from 0 to 80 ka.

A possible interpretation of these data is that river which headwaters are in formerly glaciated areas (Tinée, Vésubie) incise faster during and after the LGM not only because of increasing precipitations but also because of the massive release of glacier meltwaters occurring at that time (e.g. Saillard et al., 2014; Rolland et al., 2020). More recently, Cardinal et al. (2022) have

https://doi.org/10.5194/egusphere-2022-709
Preprint. Discussion started: 10 August 2022

suggested a complex response of river systems of the SW French Alps to deglaciations, depending on their connection with glaciated areas and on the presence of lithological knickpoints.

To summarize, these data suggest: 1) transient, post-YD and very fast incision in high altitude areas; 2) steady, fast incision rates at ~1 $\mathrm{mm.yr^{-1}}$ since the last 15-20 ka in almost all other points; 3) lower incision rates of ~0.2 to 0.5 $\mathrm{mm.yr^{-1}}$ in the Paillon and Roya Rivers, east of the Var catchment. Whatever the catchment, it appears that data points in the last ~20 ka range along slopes that define larger incision rates (sometimes by 1 order of magnitude) than average catchment denudation rates estimated from detrital ^{10}Be in river sands or marine sediments (Mariotti et al., 2019, 2021).

3 Methods

3.1 Landscape evolution model

We use the Landscape Evolution Model (LEM) Badlands (Salles, 2016) to simulate erosion and deposition on an irregular TIN topographic grid under various tectonic (uplift) and climatic (precipitation, hillslope processes) time and space parameters. River incision is simulated using the Stream Power Law (Whipple and Tucker, 1999):

$$E = KA^m S^n \tag{2}$$

where *E* is the erosion rate $[L.T^{-1}]$, *K* is a dimensional coefficient that describes the erosional efficiency $[L^{1-2m}.T^{-1}]$, *A* is the drainage area $[L^2]$, *S* is the channel slope, *m* and *n* are positive exponents. Hillslope processes on land and at sea are simulated by a linear or non-linear diffusion law:

$$\frac{dh}{dt} = K_D \nabla^2 h \tag{3}$$

where *dh/dt* is the altitude change due to diffusive processes $[L.T^{-1}]$, *h* is the altitude $[L]$ and K_D is the hillslope diffusion coefficient $[L^2.T^{-1}]$, which can vary between the continental and marine domains. For river systems, sediment deposition occurs either when the channel slope falls below a given threshold (alluvial plain deposition) or when the rivers reach their baselevel. In addition, we take into account submarine sediment transport in order to simulate the occurrence of hyperpycnal flows. Following an approach similar to Petit et al. (2015) and Thran et al. (2020), we assume that hyperpycnal flows occur when the sediment load at the river mouth is larger than a given threshold. If the flow density exceeds this threshold, instead of being deposited near the baselevel, sediments continue their route along the submarine slope. In addition, we assume that the flow does not incorporate water along its path. The flow density at the river mouth $[M.L^{-3}]$ can be computed: i) either with a mass estimate from water and sediment discharge (Q_w and Q_s, respectively $[L^3.T^{-1}]$) and densities (ρ_w ans ρ_s, respectively):

$$\rho_f = \frac{\rho_w.Q_w + \rho_s.Q_s}{Q_w + Q_s} \tag{4}$$

or using the rating parameters *a* and *b* (Syvitski et al., 2000), which can be determined for each river system from discharge and sediment load measurements. Submarine flow may trigger bedrock erosion as for aerial channels, but the parameters of the stream power law are adjusted in order to account for: 1) constant drainage area along channel length in the submarine domain

https://doi.org/10.5194/egusphere-2022-709
Preprint. Discussion started: 10 August 2022

and 2) lower shear stress on the submarine channel bed compared to aerial rivers, which is simplified assuming an effective slope S_{eff} such that:

$$S_{eff} = S\frac{\rho_s - \rho_w}{\rho_s} \quad (5)$$

Deposition occurs in the submarine domain either for gentle slopes (similar to alluvial plains on land) and beneath a certain depth corresponding to the depth of the abyssal plain. Flexural isostasy can be incorporated with a constant or space-variable effective elastic thickness (EET) used to compute the vertical motion resulting from the response of the lithosphere to loading (by ice, sedimentation or sea level rise) or unloading (deglaciation, erosion or sea level drop).

3.2 Ice cover and sea level changes

As the Mercantour massif was periodically covered by glaciers during the Quaternary, we simulate the ice thickness and extent at every time step assuming that the LGM corresponds to the maximum ice extent map (Brisset et al., 2015). We consider that ice thickness varies with Mediterranean sea surface temperatures (SST), which ranged between ~5°C (LGM) and ~15°C during the considered time period (Hayes et al., 2015; Rodrigo-Gamiz et al., 2013). Glacial periods with full ice extent are imposed for SST lower than 6.5°C and complete deglaciation for SST above 11°C. Between these thresholds, the ice thickness is assumed to vary linearly with the SST. In order to avoid fast variations of the ice cover, the SST curve is smoothed using a 5 kyr sampling interval which is then resampled at 1 kyr step using cubic interpolation (3). When ice thaws, an equivalent amount of water (assuming a ratio between the ice and water heights of 0.93) is released and participates to runoff. Sea level variations can be imposed according to the Mediterranean eustatic sea level curve published in Waelbroeck et al. (2002). Badlands does not simulate glacial erosion; however, we must consider a non-null erosion rate beneath glaciated areas in order to avoid over-estimation of the ^{10}Be concentration in sediments produced by basement erosion after glaciers retreat. For this purpose, we simulate the in-situ erosion and sediment production due to glacial processes by increasing the local hillslope diffusion coefficient proportionally to the ice thickness, which will locally enhance denudation beneath glaciated areas, while river discharge is set to zero. Besides erosion, the effect of ice coverage is twofold: it blocks cosmic radiations so ^{10}Be production is null beneath in areas covered by glaciers, and it creates a positive vertical load and downward flexure of the lithosphere.

3.3 ^{10}Be production and transport

^{10}Be production rates by neutron spallation and muon capture are computed according to Braucher et al. (2011) for a latitude of 40° (Table 1) using the scaling parameters by Stone (2000) for latitude (40°) and altitude. Earth magnetic field variations are not considered in this study. The topographic shielding is computed from the TIN topographic grid. A shielding correction can be applied to account for the topographic smoothing due to the DEM resolution, which tends to underestimate the actual shielding (Norton and Vanacker, 2009).

A map of quartz-bearing rocks is defined according the geological map of Nice and its hinterland (Rouire et al., 1980); most quartz-bearing rocks correspond either to granitic and metamorphic Palaeozoic basement rocks in the Mercantour massif or to Cenozoic sandstones in the sedimentary cover (1). The average quartz concentration in source rocks is fixed at 50%. The

https://doi.org/10.5194/egusphere-2022-709
Preprint. Discussion started: 10 August 2022

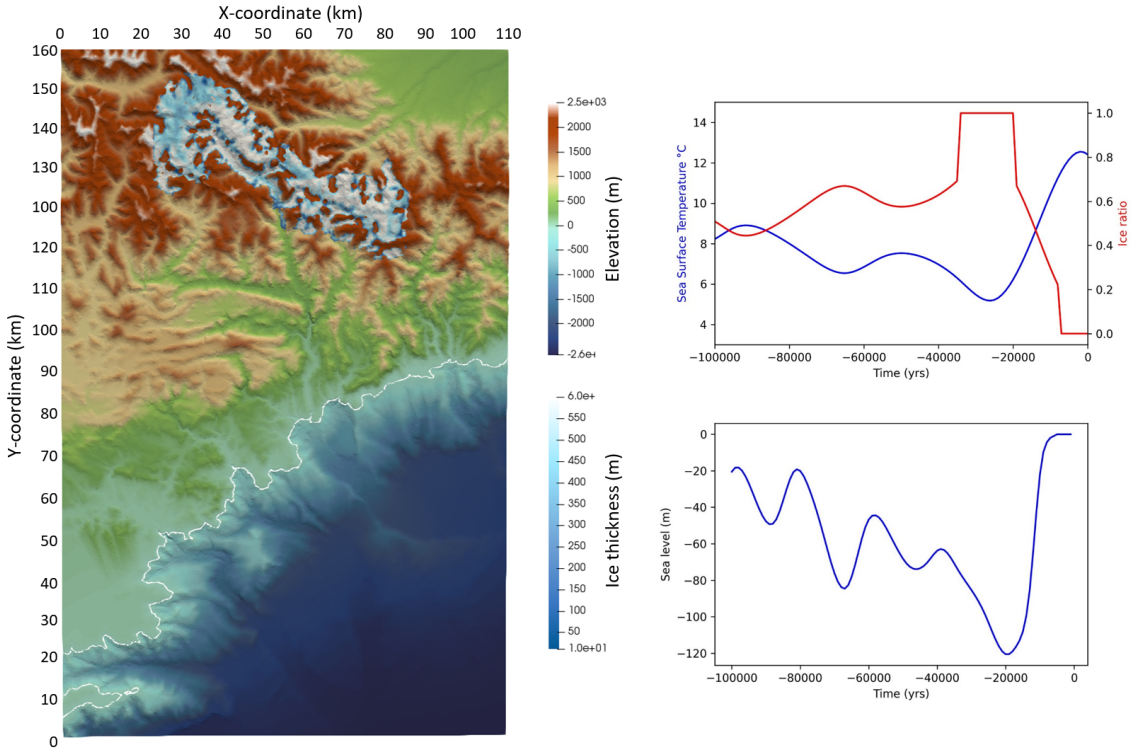

Figure 3. Left : Topography, bathymetry and maximum ice thickness (after Brisset et al., 2015); Top right: smoothed variations of the sea surface temperature (SST, after Hayes et al., 2005 and Rodrigo-Gamiz et al., 2013) in blue and ice thickness ratio (1 is for full ice, 0 for no ice) in red; bottom right: sea level variations (after Waelbroeck et al., 2002).

initial ^{10}Be concentration in quartz-bearing rocks is computed assuming a steady-state average denudation rate for the whole grid. ^{10}Be concentration *N(z,t)* varies with time and depth, and we simply compute it at the surface (z=0) of eroded domains:

$$\frac{dN(0,t)}{dt} = P(0,t) - \left(\lambda + \frac{\rho.\epsilon(t)}{\Lambda}\right) N(0,t) \tag{6}$$

where is the ^{10}Be concentration ($\mathrm{at.g^{-1}}$),is the production rate ($\mathrm{at.g^{-1}.yr^{-1}}$),is the ^{10}Be radioactive decay constant ($\mathrm{yr^{-1}}$),the rock density ($\mathrm{g.cm^{-3}}$),is the attenuation length ($\mathrm{g.cm^{-2}}$),and the erosion rate ($\mathrm{cm.yr^{-1}}$).

^{10}Be production results primarily from neutron spallation, and fast and slow muon capture with different production rates and attenuation lengths (Braucher et al., 2011) (Table 1). Assuming that erosion and production rates are constant during a given time step of the model, we can compute explicitly the ^{10}Be concentration in each eroded node of the source rocks at each time step, without any a priori steady-state assumption (Knudsen et al., 2019):

$$N(0,t) = \exp\left(\lambda + \frac{\rho.\epsilon(t)}{\Lambda}\Delta t\right).\left(N(0,t-\Delta t) + P(0,t)\frac{1}{\lambda + \frac{\rho.\epsilon(t)}{\Lambda}}\left[\exp\left(\lambda + \frac{\rho.\epsilon(t)}{\Lambda}\Delta t\right) - 1\right]\right) \tag{7}$$

For the initial ^{10}Be concentration N(0,0) we assume steady-state between ^{10}Be production and erosion by imposing a mean

https://doi.org/10.5194/egusphere-2022-709
Preprint. Discussion started: 10 August 2022

long-term erosion rate :

$$N(0,0) = \frac{P(0,0)}{\frac{\rho.\epsilon_0}{\Lambda} + \lambda} \quad (8)$$

In the case of deposited sediments, we compute the mean detrital ^{10}Be concentration and quartz content of sediments, knowing the volume contribution, quartz proportion and ^{10}Be concentration of each eroded source to the total amount of deposited sediments, assuming a perfect mixing between all sources. We use as initial conditions a smoothed topographic and bathymetric DEM with a spatial resolution of 500 m x 500 m.

In a first test, a simulation is run with a constant precipitation rate of 0.5 $\mathrm{mm.yr}^{-1}$ over 5000 years with a timestep of 100 years in order to calibrate our initial parameters against the results of Mariotti et al. (2019). More specifically, we evaluate ^{10}Be production rate in the Mercantour massif, ^{10}Be concentration in river sediments and computed denudation rates in sub-catchments of the Var drainage network, with a mean steady-state denudation rate of 0.2 $\mathrm{mm.yr}^{-1}$ (4)(Table 2). Although the model fit is not quite perfect, it allows us to verify that we get correct estimates of ^{10}Be production and erosion rates. Only the data from the Coulomp River, a small tributary of the Var River, could not be satisfyingly reproduced (Table 2 - Cou16-1), where the predicted low ^{10}Be concentration resulted in a denudation rate more than twice as high as in Mariotti et al. (2019).

Table 1. Sea level high latitude parameters for ^{10}Be production (after Braucher et al. (2011))

Neutron spallation rate $at.g^{-1}.a^{-1}$	Slow muon capture rate $at.g^{-1}.a^{-1}$	Fast muon capture rate $at.g^{-1}.a^{-1}$	Neutron attenuation length $g.cm^{-2}$	Slow muon attenuation length $g.cm^{-2}$	Fast muon attenuation length $g.cm^{-2}$	Radioactive decay constant a^{-1}	Density $g.cm^{-2}$
4.49	0.012	0.039	160	1500	4320	4.9867e-7	2.5

Table 2. Calibration of ^{10}Be production and erosion rates after the results of Mariotti et al. (2019) for the present-day rates

Sample site	Production rate $at.g^{-1}.yr-1$		^{10}Be concentration $at.g^{-1}$		Erosion rate $mm.yr^{-1}$	
	M2019	This study	M2019	This study	M2019	This study
Tin16-1	18.793	21.626	(3.17±0.67)e4	3.67e4	0.38±0.08	0.31
Tin16-2	17.539	19.452	(4.16±0.11)e4	3.67e4	0.27±0.07	0.30
Ves16-1	20.408	20.747	(2.3±0.36)e4	3.30e4	0.57±0.09	0.23
Ves16-2	17.971	16.025	(3.32±0.68)e4	3.40e4	0.35±0.07	0.22
Var16-3	17.392	17.257	(3.44±0.80)e4	4.00e4	0.33±0.08	0.25
Est16-1	7.787	8.414	(3.29±0.63)e4	3.14e4	0.16±0.03	0.16
Cou16-1	12.714	12.622	(8.03±0.11)e4	3.08e4	0.10±0.08	0.24

https://doi.org/10.5194/egusphere-2022-709
Preprint. Discussion started: 10 August 2022

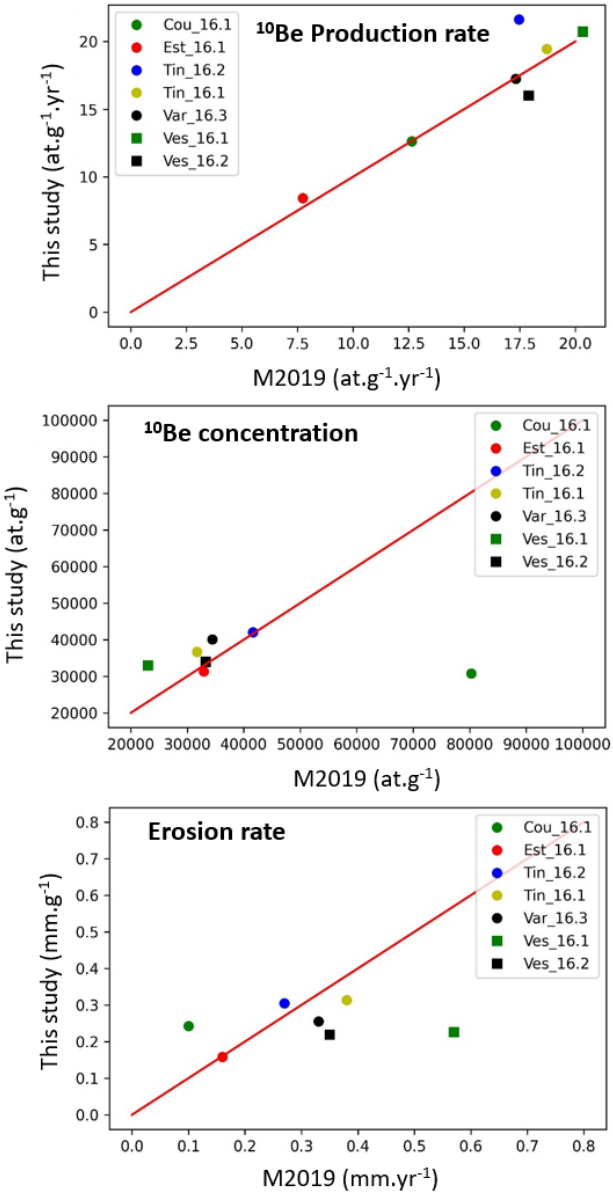

Figure 4. Comparison between the results of Mariotti et al. (2019) (x-axis) and the short-term model (this study, y-axis) for several rivers of the Var catchment, for ^{10}Be production rates (top), ^{10}Be concentration in river sediments (middle) and steady-state erosion rates (bottom). Red line indicates the 1:1 slope. See Table 2 for values.

https://doi.org/10.5194/egusphere-2022-709
Preprint. Discussion started: 10 August 2022

4 Results

4.1 Record of time variable erosion rates in river sands and at sea

We then test the response of a topographic grid representing the Var aerial and submarine systems to climatic (precipitation) variations. The model runs for 100 kyr with an adaptive time step of max. 1000 years. We keep a constant rock erodibility of 5e-6 $\mathrm{m}^{1-2\mathrm{m}}.\mathrm{yr}^{-1}$ and a hillslope diffusion coefficient of 2.5e-2 $\mathrm{m}^2.\mathrm{yr}^{-1}$. The river sediment load is computed from water discharge using rating parameters (Syvitski et al., 2000) for the Var River *a* and *b* equal to 1.e-3 and 1.6, respectively, and a low threshold density (i.e., equal to water density), which insures that all river sediments are exported to the deep submarine basin and that no large river delta is formed near the coastline.

In a first series of tests, we investigate how well the ^{10}Be concentrations in continental (i.e., in river sand) and submarine (turbidite-like) deposits compare with the average catchment denudation rate directly output from the model. For this purpose, we select the total area of the Var catchment where ^{10}Be is produced and compute the average ^{10}Be concentration N_{ex} in exported sediments for each time step, from the contribution of each catchment node i such as:

$$\overline{N_{ex}} = \frac{\sum_{i=1}^{n} N_i \epsilon_i Q_i}{\sum_{i=1}^{n} \epsilon_i Q_i} \tag{9}$$

where Q_i is the quartz proportion in each node, N_i is the ^{10}Be concentration ($at.g^{-1}$) and the eroded mass of sediments (g). Then we use equation 7 to compute the catchment denudation rate assuming a steady-state condition, and compare it with the average denudation rate directly output from the model. Finally, we extract the average $^{10}\mathrm{Be}_{\mathrm{MS}}$ in an 8x8 km area located downstream of the Var submarine canyon, and use the same equation to compute the average catchment denudation rate variations as recorded by deep sea sediments (as shown in 5). Simulations are run with alternating low (0.25 $\mathrm{m.yr}^{-1}$) and high (1 $\mathrm{m.yr}^{-1}$) precipitation rate periods lasting 20 kyr each (6). The first simulation is run with a constant sea level, no ice cover and no lithospheric flexure; then we successively implement a variable Mediterranean sea-level, ice cover in the Mercantour massif (see 3) and lithospheric flexure with a constant *EET* of 20 km, which corresponds to a moderately rigid lithosphere where the crust and mantle elastic lids are decoupled (Burov and Diament, 1995). In simulations without ice cover (Figures 6A, 6B), denudation rates estimated from in-situ sediments do record the succession of periodic pulses but generally overestimate the actual denudation rate by a few percent. This overestimation reflects a more intense erosion in low-altitude river thalwegs than on the hillslopes and high-altitude interfluves, which slightly promotes the export of ^{10}Be-poor sediments with respect to ^{10}Be-rich ones, hence increasing the apparent denudation rate. In simulations computed with a transient ice cover (Figures 6C and 6D), in-situ produced sediments are less rich in ^{10}Be, due to the absence of production beneath ice, which leads to higher apparent denudation rates; this effect can easily be accounted for and corrected, provided we have a reasonably good estimate of the ice cover extent though time (Mariotti et al., 2021). In this region, the effect of ice cover is quite important (~50% of the actual denudation rate) because the ice extends precisely over the area where ^{10}Be is produced (the Mercantour crystalline massif).

For all simulations, both in-situ and actual denudation rate evolutions depict more complex patterns than the imposed climatic (precipitation) forcing. Short-period, low-amplitude variations are visible, which are related to local and internal adjustments

https://doi.org/10.5194/egusphere-2022-709
Preprint. Discussion started: 10 August 2022

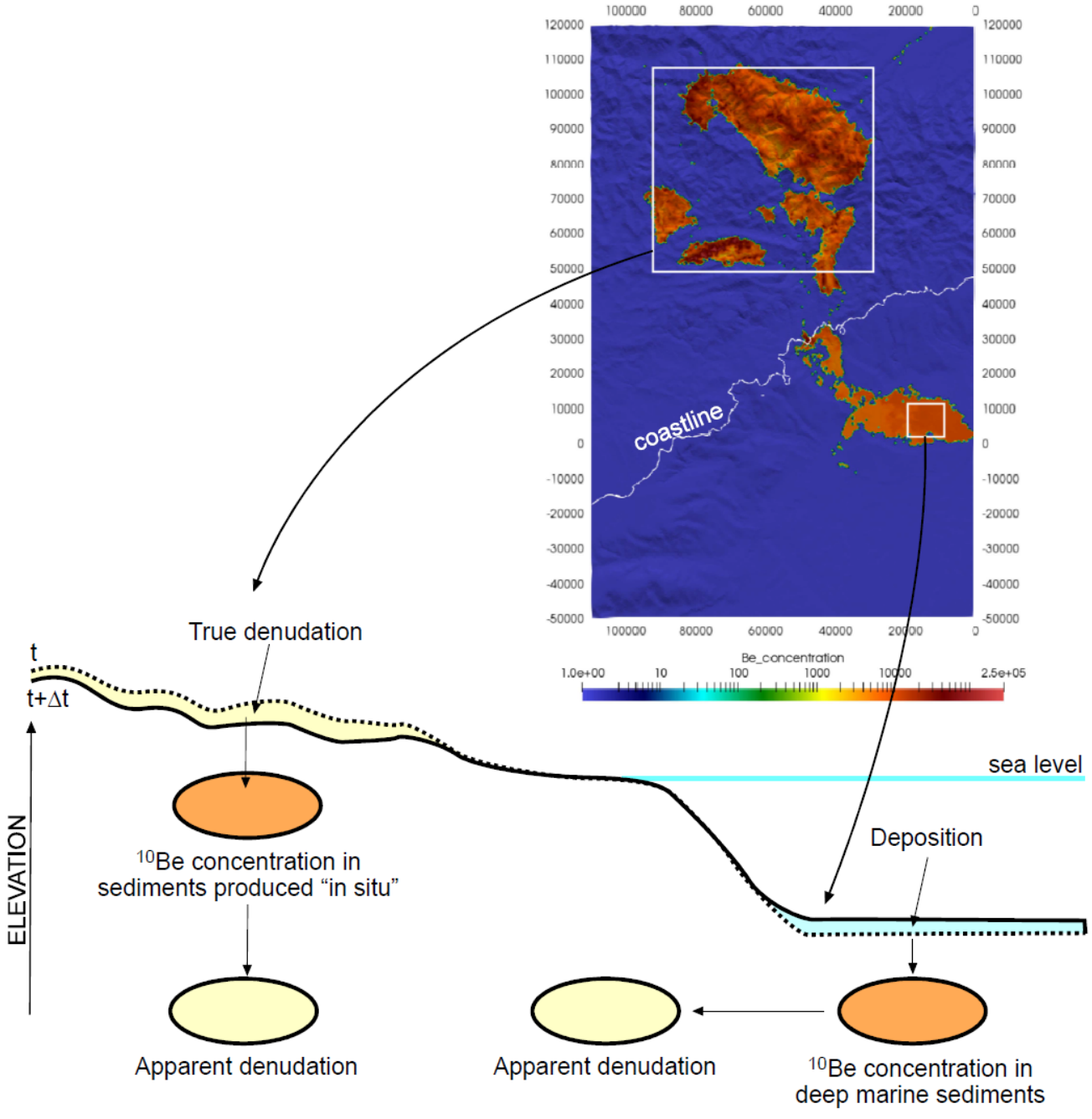

Figure 5. Computation of apparent denudation for a model time step using the mean ^{10}Be concentration of in-situ produced sediments (large square on the map, left part of the topographic profile) and the mean ^{10}Be concentration of marine sediments ($^{10}Be_{MS}$, small square on the map, right part of the profile). Map shows the ^{10}Be concentration of source rocks for a simple model with constant precipitation (0.5 $m.yr^{-1}$) after 100 kyrs.

https://doi.org/10.5194/egusphere-2022-709
Preprint. Discussion started: 10 August 2022

of the modelled topography and not to the external forcing, although sea level variations seem to amplify them (Figures 6A and 6B). There is no clear time lag between higher precipitation periods and their record in in-situ sediments, but the apparent denudation rate from in-situ river sediments displays a curved shape at the transition between low and high precipitation rate periods, which corresponds to well-known analytical solutions (Bierman and Steig, 1996). This reflects the time needed for ^{10}Be concentration to reach a steady-state relative to the massif denudation rate (~5 ka); this effect is however less visible at the transition from high to low precipitation rates.

Recording of denudation rate variations in the submarine domain is much less accurate than in local river sediments. In all runs, after a phase of model adjustment of ~10 kyr, regressive erosion reaches the highest elevations, ^{10}Be-rich sediments arrive in the submarine basin and the average apparent denudation rate oscillates around a mean value of 0.5 $\mathrm{mm.yr^{-1}}$, with some specific variations. In simulations without ice cover, despite the strong amplitude of precipitation changes, the amplitude of apparent denudation rate variations is low, although it increases when sea level changes are imposed (Figures 6A and 6B). Moreover, there is an offset of 10-15 kyr between the middle of the large precipitation periods and the peaks of apparent denudation rate in marine sediments, and the latter displays only smooth variations instead of sharp ones. Simulations with flexural isostatic response display even smoother curves than the ones without when considering the signal recorded in submarine sediments. During the largest part of the runs, where the Mercantour massif is partly covered by glaciers, the apparent denudation rate displays only low amplitude variations (it is even more stable when flexure is activated). Only after the deglaciation (from 15 ka to present), ^{10}Be-poor sediments start to feed the deepest part of the offshore basin and cause an apparent, sharp increase in denudation rates. At any given time, marine sediments therefore have a different ^{10}Be signature than in-situ produced ones, which suggests that they are constituted by a mixture of recent and ancient sediments stored in alluvial plains or in the proximal marine domain.

This series of tests seem to indicate that:

i) the alluvial deposits near the source record well the variations in the rate of denudation, although they may slightly overestimate them, unless there is (even transiently) a large ice cover over most of the quartz-bearing rock area. In these 2 latter cases, denudation rates can be overestimated by as much as 50, highlighting the critical effect of the ice sheet on the ^{10}Be concentration of high-altitude eroded rocks;

ii) detrital ^{10}Be in submarine sediments does not allow to retrieve sharp climate variations, but records an average denudation rate close to the actual long-term one (with the same error as for in-situ sediments when ice cover is present), where only smooth changes are visible;

iii) finally, there can be a significant time lag between the middle of the high precipitation period and the peak in denudation rates recorded in submarine sediments. In order to refine our understanding of the smoothing and time lag effects, we aimed at tracing artificially produced ^{10}Be-rich sediments in the submarine record. To do so, we imposed a constant, large ^{10}Be concentration in high-altitude peaks (above 1800 m) over a 5 kyr period from 30 to 35 ka. Then, we compare the ^{10}Be signature of deep-sea sediments between two identical models, one ran with the ^{10}Be peak and one without. We do not show all the tests here for the sake of simplicity, but rather illustrate a typical signature of this transient ^{10}Be peak, as visible in submarine sediments. This typical result is obtained accounting for a variable sea level, ice cover and lithospheric flexure, and a constant

https://doi.org/10.5194/egusphere-2022-709
Preprint. Discussion started: 10 August 2022

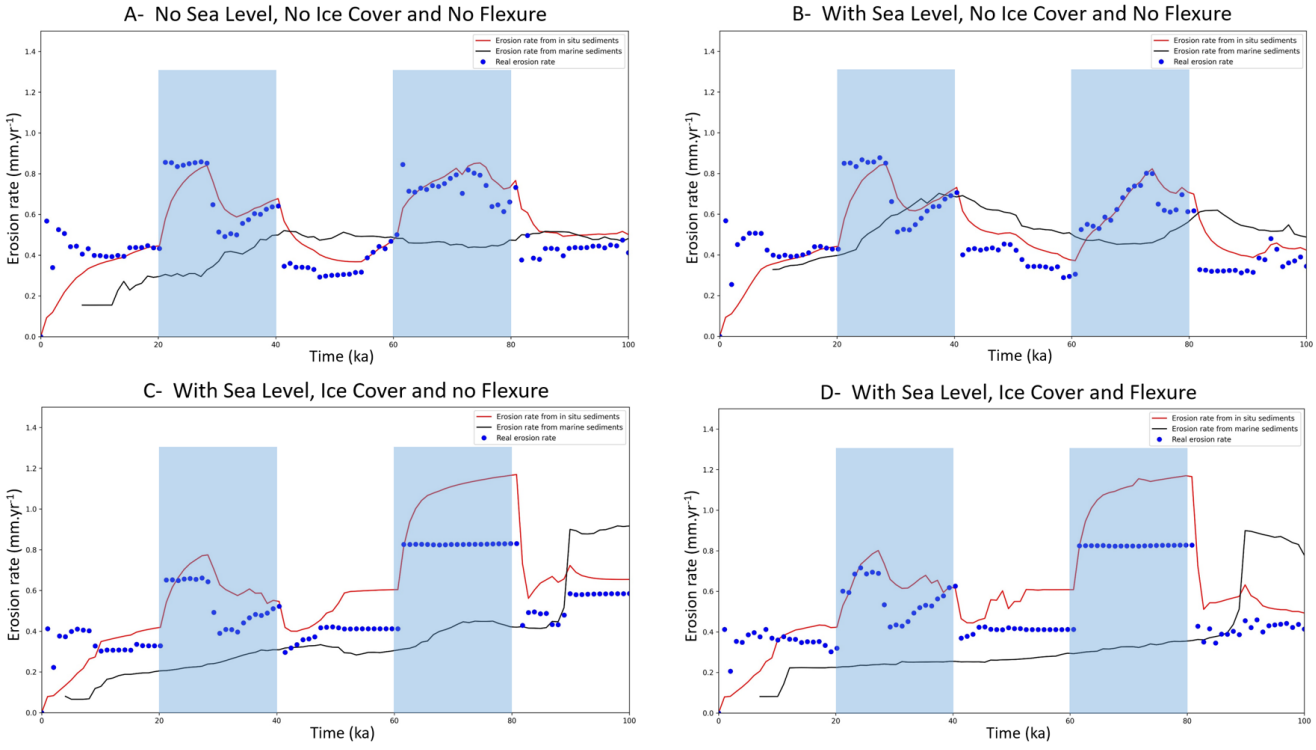

Figure 6. Test of the apparent denudation rates given by the ^{10}Be concentration of in-situ (red line) and deep sea ($^{10}Be_{MS}$, black line) sediments, versus the actual one extracted from the model (blue dots). Periods of large precipitation rates are indicated by the transparent blue rectangles. A: model with only variable precipitation rate; B: model with variable precipitation rate and sea level variations; C: model with variable precipitation rate, ice cover and sea level variations; D: model with variable precipitation rate, sea level variations, ice cover and flexure.

precipitation rate of 0.5 $\mathrm{m.yr^{-1}}$. The time lag from source to sink appears to be relatively small (1-3 kyr) and similar to the simulation presented in Figure 6D but with constant precipitation. ^{10}Be-rich sediments arrive in the basin shortly after they begin to be produced in the massif (7); however, the time lag between the onset of the ^{10}Be peak on-land and the first ^{10}Be peak recorded in marine sediments is rather large (~10-15 kyr). Moreover, this signal takes a long time to relax: sediments that are richer in ^{10}Be than the reference simulation still reach the basin ~30 kyr after the end of the production peak. These tests suggest that, although the initial time lag is not necessarily very important, the relaxation time could be so large that the submarine ^{10}Be signal could bear the superimposed effect of separate past events.

4.2 Best-fitting model for the Var catchment over the last 100 ka

Finally, we try to determine which parameters could fit the previously determined river incision rates during the last 30-40 ka in the Nice hinterland (2) and measured $^{10}Be_{MS}$ (Mariotti et al., 2021) using a trial-and-error method. We chose not to

https://doi.org/10.5194/egusphere-2022-709
Preprint. Discussion started: 10 August 2022

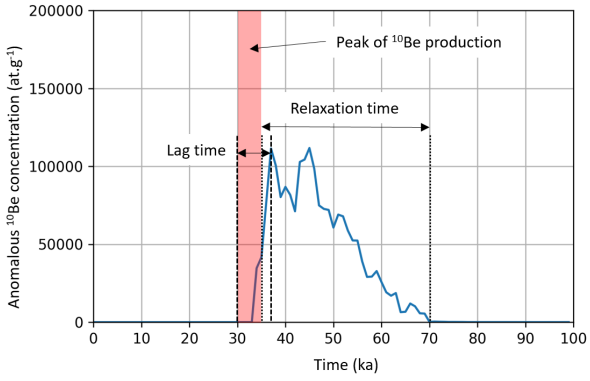

Figure 7. Difference in $^{10}Be_{MS}$ between two models with the same parameters, one having an imposed ^{10}Be-rich (2e6 $at.g^{-1}$) rocks above 1800 m between 30 and 35 ka (red transparent rectangle). The lag time (thick dashes) is defined as the interval between the onset of the 10Be peak in the massif and the age of the first ^{10}Be peak in marine sediments. The relaxation time is defined as the interval between the end of the ^{10}Be peak in the massif and the end of excess ^{10}Be recorded in marine sediments.

consider the two river gorge sites that have been dated in the upper Tinée valley (Salso Moreno and Isola, see 1), because they likely correspond to very transient post-glacial sediment wash-out that is not possible to model (Rolland et al., 2020). Initial and boundary conditions are similar to the previous series of runs. Sea level variations and ice cover are imposed, and simulations are run for 100 kyr with a time step of 1 kyr. Here again, flexural isostatic response is computed using a constant effective elastic thickness of 20 km. We first present the best-fit model obtained by evaluating the fit to river incision rates and ^{10}Be measurements, then we discuss the implications of each parameter (flexure, sea level, ice cover) in the final result. This simulation involves a precipitation rate of 0.3 $\mathrm{m.yr^{-1}}$ from 0 to 80 kyr increasing to 0.7 $\mathrm{m.yr^{-1}}$ during the last 20 kyr, an initial denudation rate of 0.2 $\mathrm{mm.yr^{-1}}$, a diffusion coefficient of 2.5e-2 $\mathrm{m^2.yr^{-1}}$ in submarine and river sediments and of 0.1 $\mathrm{m^2.yr^{-1}}$ in bedrock areas and a constant erodibility coefficient of 3.5e-6 $\mathrm{m^{1-2m}.yr^{-1}}$ (8). This model satisfyingly reproduces measured incision rates in river channels and yields a slight increase in $^{10}Be_{MS}$ in the Var deep sea fan after ~40 ka (Figure 9A). Given the large variability of $^{10}Be_{MS}$ values (as depicted by the standard error bars), the modelled $^{10}Be_{MS}$ variation is compatible with almost all measurements published in Mariotti et al. (2021). From the simulation outputs, we find that the increase in $^{10}Be_{MS}$ is not due to a change in erosion rate on land: indeed, river incision rates tend to increase after 20 ka due to the release of glacier meltwaters and to increased precipitation rates, while the $^{10}Be_{MS}$ also increases. The observed increase in $^{10}Be_{MS}$ around 40 ka is due to the presence of a patch of ^{10}Be-rich sediments deposited in the basin in the early stages of the model, which slowly migrates towards the lowest areas of the basin during the run. The simulation fit with the measured $^{10}Be_{MS}$ is somehow fortuitous, since it varies at lot, both locally and vertically. This simulation thus shows that: 1) ^{10}Be concentration at the surface of the submarine basin at a given time can be highly variable; hence, the vertical variation of $^{10}Be_{MS}$ can also be variable from one place to another, and 2) it is quite possible to get both increased incision rates on-land and apparent decreased denudation rates in submarine cores.

https://doi.org/10.5194/egusphere-2022-709
Preprint. Discussion started: 10 August 2022

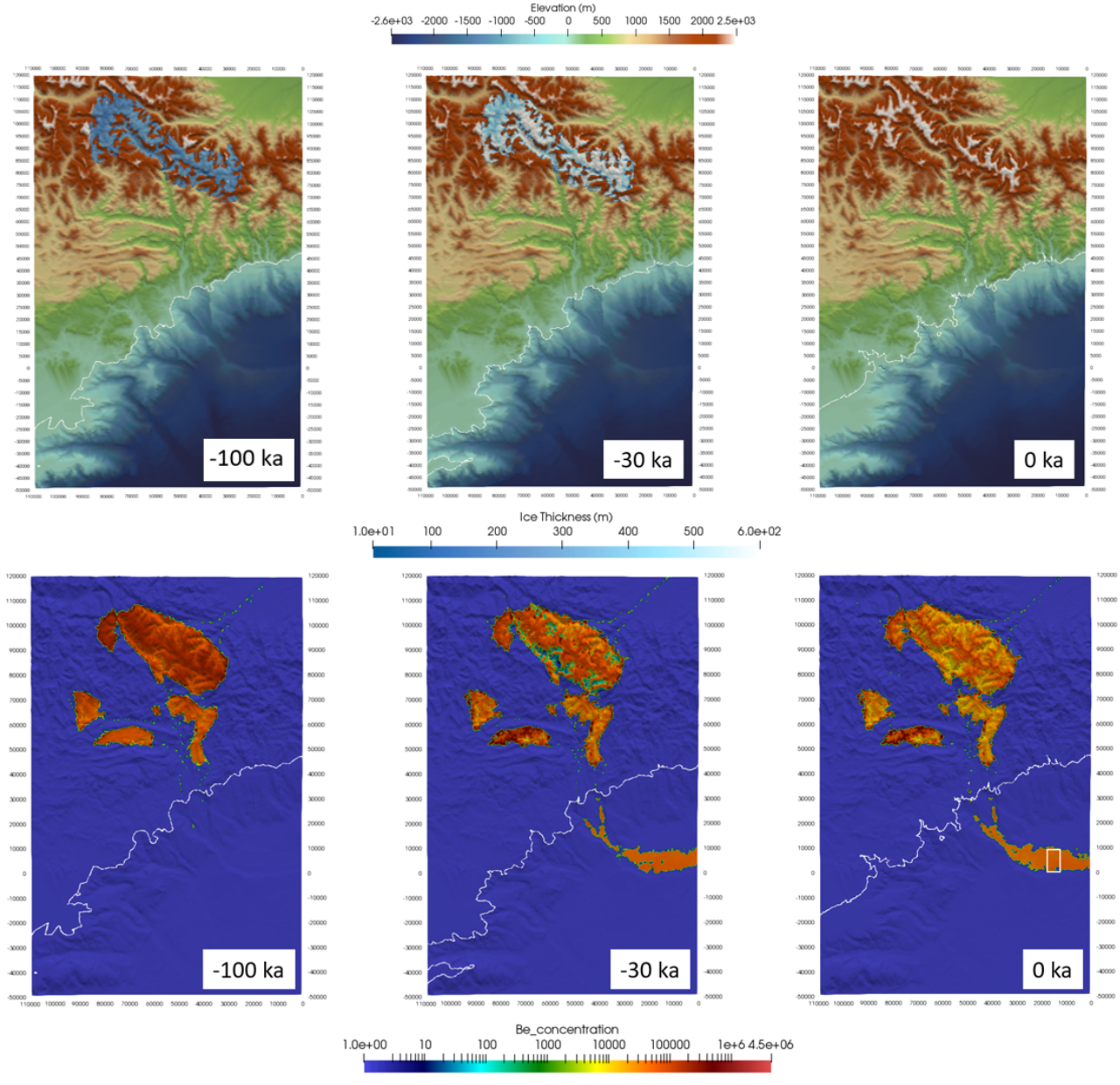

Figure 8. Stages of evolution of the best-fitting model from 0 to 100 ka (model time, corresponding to -100 to 0 ka in reality). Upper panels present the topography and ice thickness, lower panels present the surface ^{10}Be concentration. White rectangle on the lower right panel indicates the area where average $^{10}Be_{MS}$ has been computed (see results on 9).

https://doi.org/10.5194/egusphere-2022-709
Preprint. Discussion started: 10 August 2022

Starting from this reference simulation, we then evaluate the individual effects of lithospheric flexure, ice cover and sea level changes. A similar simulation without lithospheric flexure predicts slightly lower incision rates for all rivers, with a more dramatic change for the Vésubie River where it underpredict the rate by a factor of ~3 times (Figure 9B); meanwhile, both the absolute values of $^{10}Be_{MS}$ and their variations decrease below observations. A simulation similar to the reference one but without ice cover (Fig. 9C) predicts too low incision rates for some rivers (Vésubie, Estéron, Bévéra, Lower Tinée), but a good fit to $^{10}Be_{MS}$ and to some other rivers (Paillon and Roya). Removing sea level changes does not significantly affect the simulated river incision rates, but gives a lower and more stable $^{10}Be_{MS}$ signal (Figure 9D). Finally, a simulation with constant precipitation rate gives satisfying results for the rivers incision rates but too low $^{10}Be_{MS}$, although an increase is still observed after 20 ka. Although in nature, these forcings are interacting together, we can see that:

- Only simulations with sea level changes produce an increase in $^{10}Be_{MS}$ after 30-40 ka.
- The large incision rate in the Vésubie River (compared to Bévéra, Roya, Estéron and Paillon) can only be explained by the effect of isostatic rebound, the latter being smaller in the simulations with no glaciers.
- Cosmic ray exposure (CRE) data on river-polished walls do not allow to discriminate between constant (0.5 $mm.yr^{-1}$) or variable (0.3 then 0.7 $\mathrm{mm.yr^{-1}}$) precipitation rates.
- However, a constant precipitation induces more important denudation in the earliest stages of the predicted evolution (compared to the reference simulation where precipitation rate is low), hence producing on average a lower $^{10}Be_{MS}$.
- A combination of sea level changes, ice cover and lithospheric flexure provides a reasonable fit to measured $^{10}Be_{MS}$.

5 Conclusions

The Var source-to-sink sediment system is shown to be especially appropriate to trace the effect of past glaciations by cosmic ray exposure (CRE) dating, as almost all quartz-bearing rocks (i.e., rocks that produce ^{10}Be) are located in the high Mercantour massif, which was partially covered by ice during glacial periods. Clearly, if this was not the case (i.e., if quartz-bearing rocks were in low altitude areas), the effect of transient ice cover would have been less important. Therefore, for the Var catchment case, it is crucial to be able to correctly estimate the effect of the ice cover on ^{10}Be production, since it can lead to an overestimation of the actual denudation rates by as much as 50%.

Our results based on dating and modelling indicate that, while river sands do accurately estimate the average denudation rate of continental catchments for the Var region (provided the latter does not vary at high frequency, i.e., with periods smaller than the time needed to reach steady-state), it is much less the case for submarine deep-sea sediments. These sediments have a different, and often much noisier, signature than continental ones, and record significant lag and/or relaxation times with respect to external forcings, probably due to the geomorphological response of the continental margin. This area being prone to strong and rapid geomorphological modifications (i.e., transition from narrow bedrock channels to wide, braided rivers) during violent flood events (like during the Alex storm, which took place in October 2020), it could be of primordial importance to estimate the relaxation time of such events and their role on the long-term landscape evolution and geochemical signature of the sedimentary archives.

https://doi.org/10.5194/egusphere-2022-709
Preprint. Discussion started: 10 August 2022

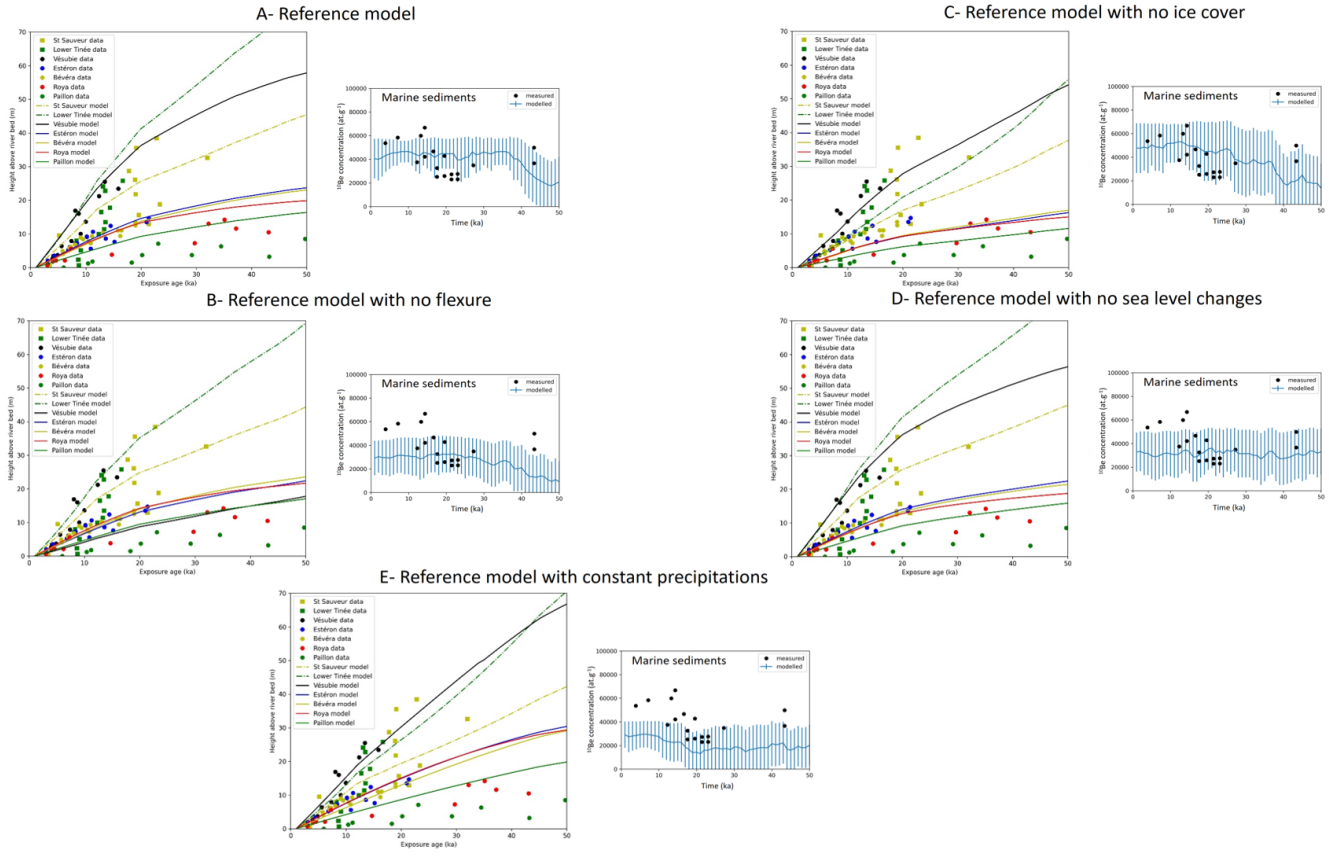

Figure 9. Comparison between model outputs and data from CRE ages in river-polished cliffs (left panels, see 2) and $^{10}Be_{MS}$ (right panels, after Mariotti et al., 2021). Vertical bars on the right correspond to measured standard deviations in $^{10}Be_{MS}$ in the sampled area (8).

On the long-term, the presence of ice in the massifs where ^{10}Be production occurs, together with the reworking of alluvial and deltaic sediments during low sea-level periods and vertical motions due to lithospheric flexure largely alter the signal coming from precipitation variations, and can lead to poor estimates of the actual denudation rate variations from $^{10}Be_{MS}$. All these effects have been exemplified in this study of the Var catchment where the distance from source to sink is short, precipitation rates are large and the mouth of the main rivers are devoid of any large deltas. Hence, in regions with very large catchments, alluvial plains and deltas, it could be even more difficult to reconstruct past denudation rates from deep sea sediments.

Our reference simulation highlights the complex interactions between river incision, sea level variations, ice coverage and the resulting isostatic response of the lithosphere. It seems impossible to disentangle the respective role of any of these forcings specifically, as most of them are interdependent. However, further tests (9) show that, depending on their location, rivers have a different sensitivity to these parameters: the Estéron, Roya, Paillon and Bévéra are less affected by the parametric changes applied to the reference forcing conditions: their incision rate is only significantly reduced when considering no sea level changes, nor ice cover or flexure (not shown here).

https://doi.org/10.5194/egusphere-2022-709
Preprint. Discussion started: 10 August 2022

Oppositely, the rivers with the largest incision rates (Vésubie and Tinée Rivers) are also the ones which seem more sensitive to the effect of ice cover and flexural isostatic response of the lithosphere (9). It is possibly because a significant part of their length (20-40) runs over the Mercantour crystalline massif, i.e. over the area where post-glacial isostatic rebound is important. The sampling sites of these rivers being rather close to their headwaters, they are not sensitive to sea level variations. Quantification of each river sensitivity to local or regional processes like isostatic uplift, sea level changes, precipitation or ice cover, depending on the dating site location, could therefore be useful to better understand the respective importance of these external forcings on this South Alpine margin.

Code and data availability. The corresponding version of Badlands with all the data used for this paper can be found here: https://github.com/badlands-model/badlands-Be

Author contributions. CP developped the implementation for Badlands, performed model runs and redaction; TS checked and released the new version of the code and participated to the redaction. VG and LA participated to the redaction

Competing interests. The authors declare no conflict of interest.

Acknowledgements. This study is part of a project that has been funded by the French Geological Survey (Bureau de Recherches Géologiques et Minières; BRGM) through the national program “Référentiel Géologique de France” (RGF-Alpes). This work has been supported by the French government, through the UCA-JEDI Investments in the Future project managed by the National Research Agency (ANR) with the reference number ANR-15-IDEX-01. Fruitful discussions with Sébastien Carretier (Toulouse) and Guillaume Duclaux (Geoazur) were greatly appreciated.

https://doi.org/10.5194/egusphere-2022-709
Preprint. Discussion started: 10 August 2022

References

Armitage, J., Dunkley Jones, T., Duller, R., Whittaker, A., and Allen, P.: Temporal buffering of climate-driven sediments flux cycles by transient catchment response, Earth and Planetary Science Letters, 369-370, 200–210, https://doi.org/10.1016/j.epsl.2013.03.020, 2013.

Balco, G., Stone, J., Lifton, N., and Dunai, T.: A complete and easily accessible means of calculating surface exposure ages or erosion rates from 10Be and 26Al measurements., Quaternary Geochronology, 3, 174–195, https://doi.org/10.1016/j.quageo.2007.12.001, 2008.

Bentley, S., Blum, M., Maloney, J., Pond, L., and Paulsell, R.: The Mississippi River source-to-sink system: Perspectives on tectonic, climatic, and anthropogenic influences, Miocene to Anthropocene, Earth-Science Reviews, 153, 139–174, https://doi.org/10.1016/j.earthscirev.2015.11.001, 2016.

Bierman, P. and Steig, E.: Estimating Rates of Denudation Using Cosmogenic Isotope Abundances in Sediment, Earth Surface Processes and Landforms, 21, 125–139, 1996.

Blöthe, J. and Korup, O.: Millennial lag times in the Himalayan sediment routing system, Earth and Planetary Science Letters, 382, 38–46, https://doi.org/10.1016/j.epsl.2013.08.044, 2013.

Bonneau, L., Toucanne, S., Bayon, G., Jorry, S., Emmanuel, L., and Silva Jacinto, R.: Glacial erosion dynamics in a small mountainous watershed (Southern French Alps): A source-to-sink approach, Earth and Planetary Science Letters, 458, 366–379, https://doi.org/10.1016/j.epsl.2016.11.004, 2016.

Braucher, R., Merchel, S., Borgomano, J., and Bourlès, D.: Production of cosmogenic radionuclides at great depth : A multi element approach, Earth and Planetary Science Letters, 309, 1–9, https://doi.org/10.1016/j.epsl.2011.06.036, 2011.

Brisset, E., Guiter, F., Miramont, C., Revel, M., Anthony, E., Delhon, Arnaud, F., E., E. M., and de Beaulieu, J.-L.: Lateglacial/Holocene environmental changes in the Mediterranean Alps inferred from lacustrine sediments, Quaternary Science Reviews, 110, 49–71, https://doi.org/10.1016/j.quascirev.2014.12.004, 2015.

Burov, E. and Diament, M.: The effective elastic thickness Te of continental lithosphere What does it really mean, Journal of Geophysical Research, 100, 3905–3297, 1995.

Cardinal, T., Rolland, Y., Petit, C., Audin, L., Zerathe, S., Schwartz, S., and the ASTER Team: Fluvial bedrock gorges as markers for Late-Quaternary tectonic and1 climatic forcing in the French Southwestern Alps, Geomorphology, submitted, 2022.

Clift, P. and Giosan, L.: Sediment fluxes and buffering in the post-glacial Indus Basin, Basin Research, 26, 369–386, https://doi.org/10.1111/bre.12038, 2014.

Fryirs, K., Brierley, G., Preston, N., and Kasai, M.: Buffers, barriers and blankets: The (dis)connectivity of catchment-scale sediment cascades, Catena, 70, 49–67, https://doi.org/10.1016/j.catena.2006.07.007, 2007.

Goren, L.: A theoretical model for fluvial channel response time during time-dependent climatic and tectonic forcing and its inverse applications, Geophysical Research Letters, 43, 10,753–10,763, https://doi.org/10.1002/2016GL070451, 2016.

Hayes, A., Kucera, M., Kallel, N., Sbaffi, L., and Rohling, E.: Lateglacial/Holocene environmental changes in the Mediterranean Alps inferred from lacustrine sediments, Quaternary Science Reviews, 110, 49–71, https://doi.org/10.1016/j.quascirev.2014.12.004, 2015.

Knudsen, M., Egholm, D., and Jansen, J.: Time-integrating cosmogenic nuclide inventories under the influence of variable erosion, exposure, and sediment mixing, Quaternary Geochronology, 51, 110–119, https://doi.org/10.1016/j.quageo.2019.02.005, 2019.

Lal, D.: Cosmic ray labeling of erosion surfaces: in situ nuclide production rates and erosion models, Earth and Planetary Science Letters, 104, 424–439, 1991.

https://doi.org/10.5194/egusphere-2022-709
Preprint. Discussion started: 10 August 2022

Li, C., Yang, S., Zhao, J., Xin, J., Dosseto, A., Bi, L., and Clark, T.: The time scale of river sediment source-to-sink processes in East Asia, Chemical Geology, 446, 138–146, https://doi.org/10.1016/j.chemgeo.2016.06.012, 2016.

Liu, Z., Zhao, Y., Colin, C., Stattegger, K., Wiesner, M., Huh, C., and Li, Y.: Source-to-sink transport processes of fluvial sediments in the South China Sea, Earth-Science Reviews, 153, 238–273, https://doi.org/10.1016/j.earthscirev.2015.08.005, 2016.

Lupker, M., Blard, P.-H., Lavé, J., France-Lanord, C., Leanni, L., Puchol, N., Charreau, J., and Bourlès, D.: 10Be-derived Himalayan denudation rates and sediment budgets in the Ganga basin, Earth and Planetary Science Letters, 333-334, 146–156, https://doi.org/10.1016/j.epsl.2012.04.020, 2012.

Malatesta, L., Avouac, J.-P., Brown, N., Breitenbach, S., Pan, J., Chevalier, M., Rhodes, E., Saint-Carlier, D., Zhang, W., Charreau, J., Lavé, J., and Blard, P.-H.: Lag and mixing during sediment transfer across the Tian Shan piedmont caused by climate-driven aggradation–incision cycles, Basin Research, 30, 613–635, https://doi.org/10.1111/j.bre.12267, 2018.

Mandal, S., Lupker, M., Burg, J.-P., Valla, P., Haghipour, N., and Christl, M.: Spatial variability of 10Be-derived erosion rates across the southern Peninsular Indian escarpment: A key to landscape evolution across passive margins, Earth and Planetary Science Letters, 425, 154–167, https://doi.org/10.1016/j.epsl.2015.05.050, 2015.

Mariotti, A., Blard, P.-H., Charreau, J., Petit, C., and Molliex, S.: Denudation systematics inferred from in situ cosmogenic 10Be concentrations in fine (50-100 µm) and medium (100-250 µm) sediments of the Var River basin, southern French Alps, Earth Surface Dynamics, 7, 1059–1074, https://doi.org/10.5194/esurf-7-1059-2019, 2019.

Mariotti, A., Blard, P.-H., Charreau, J., Toucanne, S., Jorry, S., Molliex, S., and Keddadouche, K.: Nonlinear forcing of climate on mountain denudation during glaciations, Nature Geoscience, 14, 16–22, https://doi.org/10.1038/s41561-020-00672-2, 2021.

Mulder, T., Savoye, B., Piper, D., and Syvitsky, J.: The Var submarine sedimentary system : understanding Holocene sediment delivery processes and their importance to the geological record, Geological Society of London Special Publications, 34, 145–166, 1998.

Norton, K. and Vanacker, V.: Effects of terrain smoothing on topographic shielding correction factors for cosmogenic nuclide-derived estimates of basin-averaged denudation rates, Earth Surface Processes and Landforms, 34, 145–154, https://doi.org/10.1002/j.esp.1700, 2009.

Petit, C., Migeon, S., and Coste, M.: Numerical models of continental and submarine erosion: Application to the northern Ligurian Margin, Earth Surface Processes and Landforms, 425, 681–695, https://doi.org/10.1002/j.esp.3685, 2015.

Petit, C., Rolland, Y., Braucher, R., Bourlès, D., Guillou, V., and PetitPerrin, V.: River incision and migration deduced from 36Cl cosmic-ray exposure durations: The Clue de la Cerise gorge in southern French Alps, Geomorphology, 330, 81–88, https://doi.org/10.1016/j.geomorph.2019.01.011, 2019.

Phillips, J. and Slattery, M.: Sediment storage, sea level, and sediment delivery to the ocean by coastal plain rivers, Progress in Physical Geography, 30, 513–530, https://doi.org/10.1191/0309133306pp494ra, 2006.

Rodrigo-Gamiz, M., Martinez-Ruiz, F., Rampen, S., Schouten, S., and Sinninghe Damsté, J.: Sea surface temperature variations in the western Mediterranean Sea over the last 20 kyr: A dual-organic proxy, Paleoceanography, 29, 87–98, https://doi.org/10.1002/2013PA002466, 2013.

Rolland, T., Darnault, R., Braucher, R., Bourlès, D., Petit, C., and Bouissou, S.: Deglaciation history at the Alpine-Mediterranean transition (Argentera-Mercantour, SW Alps) from 10Be dating of moraines and glacially polished bedrock, Earth Surface Processes and Landforms, 45, 393–410, https://doi.org/10.1002/esp.4740, 2020.

Rolland, Y., Petit, C., Saillard, M., Braucher, R., Bourlès, D., Darnault, R., and Cassol, D.: Inner gorges incision history: A proxy for deglaciation? Insights from Cosmic Ray Exposure dating (10Be and36Cl) of river-polished surfaces (Tinée River, SW Alps, France), Earth and Planetary Science Letters, 457, 271–281, https://doi.org/10.1016/j.epsl.2016.10.007, 2017.

https://doi.org/10.5194/egusphere-2022-709
Preprint. Discussion started: 10 August 2022

Romans, B., Castelltort, S., Covault, J., Fildani, A., and Walsh, J.: Environmental signal propagation in sedimentary systems across timescales, Earth-Science Reviews, 153, 7–29, https://doi.org/10.1016/j.earthscirev.2015.07.012, 2016.

Saillard, M., Petit, C., Rolland, Y., Braucher, R., Bourlès, D., Zerathe, S., and Jourdon, A.: Late Quaternary incision rates in the Vésubie catchment area (Southern French Alps) from in situ-produced 36 Cl cosmogenic nuclide dating: Tectonic and climatic implications, Journal of Geophysical Research: Earth Surface, 119, 1121–1135, https://doi.org/10.1002/2013JF002985, 2014.

Salles, T.: Badlands : A parallel basin and landscape dynamics model, SoftwareX, 5, 195–202, https://doi.org/10.1016/j.softx.2016.08.005, 2016.

Siame, L., Angelier, J., Godard, R. C. V., Derrieux, F., Bourlès, D., Braucher, R., Chang, K.-J., Chu, H.-T., and Lee, J.-C.: Erosion rates in an active orogen (NE-Taiwan): A confrontation of cosmogenic measurements with river suspended loads, Quaternary Geochronology, 6, 246–260, https://doi.org/10.1016/j.quageo.2010.11.003, 2011.

Syvitski, J., Morehead, M., Bahr, D., and Mulder, T.: Estimating fluvial sediment transport : The rating parameters, Water Ressources, 36, 2747–2760, 2000.

Syvitski, J., Angel, J., Saito, Y., Overeem, I., Vörösmarty, C., Wang, H., and Olago, D.: Earth's sediment cycle during the Anthropocene, Nature Review Earth and Environment, 3, 179–196, https://doi.org/10.1038/s43017-021-00253-w, 2022.

Thran, A., East, M., Webster, J., Salles, T., and Petit, C.: Theinfluence of carbonate platforms on thegeomorphological development of amixed carbonate-siliciclastic margin(Great Barrier Reef, Australia), Geochemistry, Geophysics, Geosystems, 21, https://doi.org/10.1029/2020GC008915, 2020.

Vanacker, V., von Blanckenburg, F., Hewawasam, T., and Kubik, P.: Constraining landscape development of the Sri Lankan escarpment with cosmogenic nuclides in river sediment, Earth and Planetary Science Letters, 253, 402–414, https://doi.org/10.1016/j.epsl.2006.11.003, 2007.

von Blanckenburg, F.: The control mechanisms of erosion and weathering at basin scale from cosmogenic nuclides in river sediment, Earth and Planetary Science Letters, 237, 462–479, https://doi.org/10.1016/j.epsl.2005.06.030, 2005.

Waelbroeck, C., Labeyrie, L., Michel, L., Duplessy, J., McManus, J., Lambeck, K., Balbon, E., and Labracherie, M.: Sea-level and deep water temperature changes derived from benthic foraminifera isotopic records, Quaternary Science Reviews, 21, 295–305, https://doi.org/10.1016/S0277-3791(01)00101-9, 2002.

Wan, S., Li, A., Clift, P., and Jiang, H.: Development of the East Asian summer monsoon: Evidence from the sediment record in the South China Sea since 8.5 Ma, Palaeogeography, Palaeoclimatology, Palaeoecology, 241, 139–159, https://doi.org/10.1016/j.palaeo.2006.06.013, 2006.

Whipple, K. and Tucker, G.: Dynamics of the stream-power river incision model: Implications for height limits of mountain ranges, landscape response timescales, and research needs, Journal of Geophysical Research, 104, 17,661–17,674, 1999.